

PI 3-kinase isoform p110 α controls smooth muscle cell functionality and protects against aortic aneurysm formation

Marius Vantler^{1,2,3}, Maximilian Schorsch^{1,2,3}, Eva Maria Berghausen^{1,2,3}, Joseph B. Moore IV⁴, Dickson Wong⁵, Li Zhaolong⁶, Max Wißmüller^{1,2,3}, Leoni Gnatzy-Feik^{1,2,3}, Mario Zierden^{1,2,3}, Dennis Mehrkens^{1,2}, Matti Adam^{1,2}, Xinlei Zhao⁷, Margarete Odenthal⁷, Gerhard Sengle⁹, Peter Boor⁵, Lars Maegdefessel⁶, Stephan Baldus^{1,2,3}, Stephan Rosenkranz^{1,2,3}

¹Clinic III for Internal Medicine (Dept. of Cardiology), Heart Center at the University Hospital Cologne, Cologne, Germany

²Cologne Cardiovascular Research Center (CCRC), Heart Center at the University Hospital Cologne and Medical Faculty, University of Cologne, Germany

³Center for Molecular Medicine Cologne (CMMC), University of Cologne, Germany

⁴Diabetes and Obesity Center University of Louisville School of Medicine, Louisville, KY

⁵Institute of Pathology, RWTH Aachen University Hospital, Aachen, Germany.

⁶Department of Vascular and Endovascular Surgery, Technical University Munich, Munich, Germany

⁷Institute of Pathology, University Hospital Cologne, Cologne, Germany

⁸Institute for Pharmacology and Clinical Pharmacology, University Hospital, Heinrich-Heine-University Düsseldorf, Germany

⁹Children Hospital, University Hospital Cologne, Cologne, Germany

Running title: p110 α in AAA disease

Word count: 5,517 words

Address for correspondence:

Stephan Rosenkranz, MD
Klinik III für Innere Medizin
Herzzentrum der Universität zu Köln
Kerpener Str. 62
D-50937 Köln, Germany
Phone: +49-221-478-32356
FAX: +49-221-478-32355
e-mail: stephan.rosenkranz@uk-koeln.de

Abstract

Background: Catalytic class IA PI 3-kinase isoform p110 α is a crucial regulator of cellular proliferation and survival in numerous cell types. While p110 α is critically involved in pathogenic vascular remodeling, its physiological role for vascular integrity under stress conditions has not been studied. We report a protective function of smooth muscle p110 α against abdominal aortic aneurysm (AAA) formation.

Methods & Results: In mice lacking p110 α in smooth muscle cells (sm-p110 $\alpha^{-/-}$), perfusion of the infrarenal aorta with porcine pancreatic elastase (PPE) yielded substantially enhanced AAA formation compared to wild type controls. This disease phenotype is partly attributable to a subtle preexisting vascular phenotype under basal conditions, as sm-p110 $\alpha^{-/-}$ mice displayed a smaller media area, deranged aortic wall structure (detached smooth muscle cells, increased apoptotic cell death), and a diminished functional responsiveness of aortic rings to vasodilators. Furthermore, p110 α is also implicated in regenerative processes during AAA development: Whereas wild type mice showed increased media hypertrophy, neointima formation and proliferation upon PPE intervention, these vascular remodeling processes were diminished in sm-p110 $\alpha^{-/-}$ mice. Concomitantly, increased numbers of elastic fiber breaks and ECM degradation were detected in sm-p110 $\alpha^{-/-}$ aorta. Mechanistically, we found that lack of p110 α expression impaired smooth muscle cell proliferation, expression of contractile marker genes and production of elastin fibers. This phenotype largely depended on reduced phosphorylation and inactivation of FOXO1, as specific FOXO1 inhibition fully rescued proliferation of p110 $\alpha^{-/-}$ smooth muscle cells, and knockdown of FOXO1 increased expression of calponin and elastin.

Conclusions: Smooth muscle p110 α protects against AAA disease by maintaining aortic wall homeostasis and promoting SMC proliferation to compensate for cell loss during AAA development. Our findings have potential implications for current approaches aimed at p110 α inhibition for cancer therapy and suggest new pharmacological strategies to activate p110 α signaling in AAA disease.

Key words: aortic aneurysm, PI 3-kinase, p110 α , smooth muscle cell plasticity, FOXO1

Introduction

Abdominal aortic aneurysms (AAAs) are pathological dilations of the abdominal aorta with increases of the diameters to >3 cm, or >1.5 times their normal size.^{1,2} AAA are most commonly found in the infrarenal abdominal aorta, with an overall prevalence of 6% in men and 1.6% in women.^{3,4} Unless AAAs rapidly increase in size, acutely rupture, or thromboembolize into the distal arteries, they remain clinically asymptomatic and their assessment is challenging. Fatal outcome due to rupture occurs when the intraluminal pressure and wall stress exceed the strength of the aortic wall. The mortality rate is as high as 80%,^{3,5} and it is estimated that ruptured AAAs are responsible for nearly 15,000 deaths in the United States per year.⁶ No effective pharmacological approach has been identified to date that can limit AAA progression or the risk of rupture in humans.⁷ Clinically, the only available treatment option remains surgical intervention, which includes open or endovascular aortic repair of the dilated aorta.⁷ A better understanding of the cellular mechanisms and regulatory networks driving AAA development and progression is mandatory to identifying novel therapeutic targets. In this context, animal models and, in particular, murine models, of AAA are an indispensable tool. Today, the porcine pancreatic elastase perfusion model (PPE) is considered the best mimicry of human AAA disease.⁸

Vascular smooth muscle cells (SMC) are localized in the medial layer of the vasculature, and are the predominant cell type within the aortic wall. Dysregulation of SMC functions is thought to contribute to AAA development and progression. Important functions of SMCs in healthy or disease conditions comprise apoptosis, proliferation, phenotypic switch, contractility, and extracellular matrix (ECM) production and degradation. Stress signals within the aortic wall, including inflammatory cell infiltration and (epi)genetic changes, can modulate the SMC phenotype (contractile or differentiated versus synthetic or dedifferentiated) and thus contribute to disease progression.⁹ Beside SMCs, ECM components including elastic fibers are a major constituent of the aortic wall, representing ≈50% of the dry weight.¹⁰ The aortic ECM comprises macromolecules, such as elastin and collagen, and serves many functions that are essential for vessel homeostasis. Damage or inappropriate remodeling of the ECM contributes to initiation and progression of AAA disease. Particularly, loss and degradation of elastin and collagen lead to weakening, dilatation, and ultimately rupture of the aortic wall.¹¹

Our previous work revealed that the catalytic class IA phosphatidylinositol 3'-kinase (PI3K) isoform p110 α is a crucial driver of SMC proliferation and migration and thus contributes to

vascular diseases including neointima formation after balloon injury and pulmonary hypertension.^{12, 13} Class IA PI3Ks signal downstream of receptor tyrosine kinases (RTKs), and consist of a regulatory p85 subunit and 1 of 3 distinct 110-kDa catalytic subunits (p110 α , p110 β , p110 δ). Class IA PI3Ks are lipid kinases generating phosphatidylinositol-3,4,5-trisphosphate (PIP3).¹⁴⁻¹⁶ PIP3 serves as a docking site for downstream signaling molecules such as AKT, which is considered the major transducer of PI3K signal relay. AKT phosphorylates numerous target proteins including major regulators of metabolism, mitogenesis and apoptosis including GSK3 β , caspase-9 or FOXO transcription factors.¹⁷

Although p110 α signaling in SMCs is implicated in various vascular diseases, its potential physiological functions regarding the maintenance of vascular integrity are largely unknown. Herein, we aimed to elucidate the role of p110 α in SMC proliferation, phenotypic modulation and ECM homeostasis in the aortic wall and its impact on AAA disease in mice.

Materials and Methods

Generation of smooth muscle-specific p110 α -deficient mice

Smooth muscle-specific p110 α deficient mice were generated by cross-breeding of homozygous PI3Kca^{flox/flox} mice¹⁸ with SM22-Cre mice (B6.Cg-Tg[Tagln-Cre]1Her/J, The Jackson Laboratory), which express Cre recombinase under the control of the mouse transgelin (smooth muscle protein 22-alpha) promoter. SM22-Cre^{+/-}/p110 α ^{fl/+} mice were crossed to homozygous p110 α ^{fl/fl} mice to generate SM22-Cre⁻/p110 α ^{fl/fl} (sm-p110 α ^{+/+}) and SM22-Cre⁺/p110 α ^{fl/fl} (sm-p110 α ^{-/-}) littermates.¹³ Genotyping was performed by PCR using tail biopsies.

PPE perfusion model

To induce murine AAA, the PPE infusion model was performed as described elsewhere.¹⁹ Briefly, anesthetized adult male mice (weight approx. 25-30 g) undergo a median laparotomy and the abdominal aorta is isolated at the level of the bifurcation and the left renal vein. All aortic branches within 1.0 cm of the bifurcation are ligated. Temporary ligatures are then placed around the proximal and distal aorta. An aortomy in the region of the bifurcation is then performed. A syringe pump was used to infuse the aorta 100mmHg with saline or saline solution containing 0.04 U / ml of type I porcine pancreatic elastin (Sigma-Aldrich). The perfusion catheter is then removed and the aortomy was repaired without narrowing of the aorta. The induced AAA aortic segment (area between the left renal artery and the bifurcation) were harvested at 0, 3, 7, and 28 days post-surgery: Samples were snap-frozen in liquid nitrogen and then stored at -80°C pending further processing.

Aortic diameter measurements by ultrasound imaging

At baseline, and 7, 14, 21 and 28 days after aneurysm induction, ultrasound imaging was performed to assess the abdominal aortic diameter. Mice were anesthetized with continuously delivered 2% isoflurane gas inhalation. Ultrasound gel was applied to the depilated skin of the abdomen and imaging was performed with a Vevo3100 imaging system (VisualSonics). B-mode, M-mode and EKV recordings were performed using a MX550D linear array transducer (25-55 MHz, Centre Transmit: 40 MHz, Axial Resolution: 40 μ m) with a frame

rate of 230–400 frames/s. All ultrasound images were analyzed using the Vevo 3100-software and parameters like aortic diameter were calculated.

Isometric force measurements

Isometric force measurements were performed as described.²⁰ Briefly, mice were anesthetized with isoflurane and after thoracotomy, explanted sections of the aortas were immediately kept in Krebs-Henseleit buffer on ice. 2-mm segments were mounted onto steel wires connected to force transducers of a standard organ bath filled with 25 ml Krebs-Henseleit buffer at 37°C and gassed with carbogen. Each ring was equilibrated for 30 minutes and continuously stretched up to a tension of 1.1 g. KCl (80 mM) was added twice to each bath with subsequent washing. To create a dose-response curve to PGF2 α , we added it to the bath with concentration (in μ M) of 0.1, 0.2, 0.4, 1, 2, 4, and 10. Thereafter, a dose responses to acetylcholine (Ach) or nitroglycerine (NTG) were recorded with concentrations from 1×10^{-9} M in steps of half log₁₀ levels up to a concentration of $1 \times 10^{-5.5}$ M.

Bulk RNAseq

After total RNA was extracted, RNA purity and integrity were checked by microfluidic electrophoresis using the Bioanalyzer (Qiagen, Hilden Germany). Following the quality control procedure, mRNA was enriched using Oligo(dT) magnetic beads and randomly fragmented for cDNA synthesis as previously described. Libraries were generated using the NEBNext Ultra™ RNA Library Prep Kit (New England Biolabs, Ipswich, MA, USA) for the Illumina system following the manufacturer's instructions. After cluster generation, single-end sequencing was performed using the Illumina HiSeq 2500 platform. Adapters were trimmed from raw reads, which were subsequently filtered by removing reads with a low quality score (50% bases of the read is ≤ 5). To accomplish the alignment, read mapping to the hg18 reference genome was carried out by means of STAR. Then htseq-count was used to quantify mapped reads counts for every gene of each sample. Number of mapped reads were calculated and gene expression levels were presented as FPKM (Fragments Per Kilo bases per Million reads). Subsequently, the differential expression and sample distance of two conditions was calculated using the DESeq2 R package. And top 100 DE genes ordered by p-value were selected to reflect relative expression levels across samples using heatmap.

RNA-seq profiles were generated from 16 human samples (3 healthy samples and 13 diseased samples) and 8 murine samples (4 sm-p110 $\alpha^{+/+}$ samples and 4 sm-p110 $\alpha^{-/-}$ samples). Thus, in total 16 human samples and 8 murine samples were assessed for transcriptomic changes. Differentially expressed genes (DEGs) were identified using a statistical threshold of $P < 0.05$ and fold change ≥ 2 .

Cell Culture and treatment with siRNAs.

Murine SMCs were isolated from thoracic and abdominal aorta by enzymatic dispersion as described.¹³ Animals were sacrificed and the aorta was dissected, removed, and incubated with 1 ml enzyme solution (1 mg/ml Collagenase Type I, 0.3 mg Elastase, 0.3 mg Trypsin inhibitor in DMEM / 20% FBS) for 15 minutes to detach the adventitia. The remaining adventitia was removed using anatomic forceps, and the endothelium was gently removed by scraping the luminal surface. The aorta was cut into smaller pieces and incubated for further 90 minutes at 37°C in the enzyme solution to disintegrate the tissue and separate the SMCs. After centrifugation, the cell pellet was resuspended in DMEM culture medium containing 20% FCS and 1% Penicillin/Streptomycin. Cells were transferred into a well of a 24 well plate. After 2 days most of the cells were attached to the plate. Culture medium was changed after three days. After reaching 80% confluence, cells were expanded. SMCs were grown in a 5% CO₂ atmosphere at 37°C in DMEM supplemented with 100 U/ml penicillin, 100 μ g/ml streptomycin, 1% nonessential amino acids (100X), and 10% FCS.

Murine aortic SMCs in 12-well plates were transfected with 150ng siRNA (FlexiTube GeneSolution GS56458 for Foxo1, FlexiTube GeneSolution GS56484 for Foxo3, and FlexiTube GeneSolution GS54601 for Foxo4; Qiagen), respectively, according to the transfection-protocol of primary smooth muscle cells with siRNA using HiPerFect Transfection Reagent according to the manufacturer's instructions (Qiagen).

In vitro elastic fiber matrix analysis

SMCs (1×10^5) were seeded on 12 mm round coverslips in a 24-well plate and grown for seven days in 20% FCS/DMEM. Cells were fixed (4% PFA/PBS for 10 min at 37 °C) and blocked with 1% BSA/1xPBS. SMCs were permeabilized and primary antibodies diluted in blocking solution were added to the 24-well plate cover slip and incubated for 1h at RT. After 3x washing in 1xPBS, incubation with the corresponding fluorescence-coupled secondary antibody (Anti-

rabbit IgG Alexa Fluor 555 Conjugate #4413; 1:1000 diluted in 1% BSA/PBS + 0,3% TritonX100) was performed for 45 min at RT. In addition, DAPI (4,6-diamidine-2-phenylindole dihydrochloride) was added. The coverslips were then washed and mounted on slides with DAKO mount medium. Cells were washed with PBS containing 3% Triton X-100. Images were taken with a fluorescence (Axiophot, Zeiss) or confocal laser scanning microscope (SP5, Leica). Resultant SHG images were subjected to computational analyses using MATLAB software framework packages, CurveAlign and CT-FIRE as described.²¹

Proliferation assay

Real-time assessment of cell status was carried out with an IncuCyte Zoom System (Sartorius, Goettingen, Germany), as previously described^{1,22} Images were auto-collected and analyzed by using the IncuCyte software package. The cells were seeded into a 48-well plate (14000cells/well). Data standardization method: All data are normalized with the cell confluence of 0h. For example: the cell confluence (initial cell confluence) of well A is 20% at 0 hours, 40% at 3 hours, and 60% at 6 hours. The normalized cell confluence at 0h is 1, 3h is 2, and 6h is 3.

BrdU incorporation

DNA synthesis was measured by a BrdU-incorporation assay. Cells were cultured in 96-well plates (1×10^4 cells per well) in DMEM containing 20% FCS for 24 hours, washed with PBS, and starved in DMEM for 24 hours. Subsequently, cells were preincubated with the specific FOXO1 inhibitor AS1842856 (1 μ M) for 60 minutes followed by growth factor stimulation for 24 hours. BrdU incorporation was carried out according to the manufacturer's specifications (Cell Proliferation ELISA, Roche) with an incubation time of 5 hours as previously described.²³ Quantification was performed by measuring the absorbance using Power Wave 340 ELISA reader from Bio-Tek.

Immunoblotting

Quiescent SMCs were left resting or stimulated with growth factors as indicated. Cells were washed twice with HEPES/sodium chloride (20 mM HEPES, pH 7.4, 150 mM NaCl), and then lysed in extraction buffer (10 mM Tris-HCl, pH 7.4, 5 mM EDTA, 50 mM NaCl, 50 mM NaF, 1% Triton X-100, 0.1% BSA, 20 μ g/mL aprotinin, 2 mM Na₃VO₄, 1 mM PMSF). Lysates were

centrifuged (20 minutes, 12,000g), and the supernatants were subjected to Western blot analysis. Similarly, tissue samples were homogenized in RIPA buffer. Protein concentration was assessed by either the Bradford Assay or NanoDrop quantification. Homogenates were suspended in 4 × SDS sample buffer. Equal amounts of protein lysates were run on SDS–PAGE and transferred to PVDF membranes. Blots were probed with the indicated antibodies.

Immunohistochemistry & histochemistry

Explanted aortae were fixed in 4% phosphate-buffered paraformaldehyde (Santa Cruz Biotechnology). The samples were embedded in paraffin and 3 µm sections were obtained from fixed tissue blocks. Immunohistochemistry was performed using antibodies directed against the phosphorylated AKT (Cell Signaling Technology, catalog 3777) with 3,3'-diaminobenzidine as a substrate (DAB Substrate Kit, Linaris). Negative controls were performed with the omission of the primary antibody. Hematoxylin was used to counterstain. Tissue sections were stained for PCNA (Santa Cruz Biotechnology, sc-7907) to detect proliferation.

Aortic sections were stained with Picro-sirius red (Sigma Aldrich; Merck) for 1 h at room temperature to visualize collagen fibers and washed with 1% acetic acid twice for 10 min at room temperature. Measurements were made using the QuPath image analysis software to measure the amount of red-orange and yellow-green color relative to the aortic area.

For elastin, aortic sections were stained with Verhoeff's hematoxylin for 1 h, differentiated in 2% ferric chloride for 2 min and counterstained with Van Gieson solution for 5 min (all at room temperature) to identify elastic fibers in the aortic tissue. For analysis, a scoring system between 1 and 4 was used as described elsewhere²⁴: (1) intact elastin layer; (2) mild degradation of elastin and some laminar disruption or rupture; (3) moderate elastin degradation and multiple interruptions or breaks in the lamina; (4) severe elastin breakdown or loss or aortic rupture.

Real-time qPCR

Briefly, aortae were isolated and homogenized using Precellys Lysing Kit (Bertin technologies) and Qiashredder (Qiagen). Total RNA from aortae was isolated with RNeasy micro kit (QIAGEN). cDNA was prepared with SuperScript III first-strand synthesis system (Invitrogen).

qRT-PCR of Foxo1, Acta2, Cnn1, Eln, Col1a1, Mmp2, Mmp9, and Gapdh genes was performed using TaqMan gene expression assays (Applied Biosystems).

Materials and antibodies

Chemicals were obtained from Sigma-Aldrich Chemie GmbH. Rat tail collagen type I was obtained from BD Biosciences, elastase from Serva Electrophoresis GmbH, and collagenase from Sigma-Aldrich Chemie GmbH. The antibody against RasGAP (clone 69.3) was a gift from Andrius Kazlauskas (University of Illinois, Chicago, U.S.) and the fibrillin-1 antibody was kindly provided by G. Sengle (University Hospital of Cologne, Germany). The phospho-Akt Thr308 (catalog 13038), phospho-AKT1 (catalog 9018), phospho-AKT2 (catalog 8599), phospho-GSK3 β (catalog 9322), phospho-FOXO 1&3 (catalog 9496), phospho-FOXO4 (catalog 9471), p110 α (catalog 4255), calponin (catalog 17819), PCNA (catalog 13110), and anti-rabbit IgG (H+L), F(ab')₂ Fragment (Alexa Fluor[®] 555 Conjugate) (catalog 4413) antibodies were obtained from Cell Signaling Technology; α -actin (catalog 53141) antibody from Santa Cruz Biotechnology; β -actin (catalog ab2827) and tropoelastin (catalog ab21600) from Abcam; and Myosin-heavy-chain (catalog MAB4470) from rndsystems. PDGF-BB (catalog C-63022), Insulin (catalog C-60840) were purchased from Promo Cell. AS1842856 was from Sigma-Aldrich.

Statistics

All data are expressed as mean \pm S.D. from at least 3 independent experiments. Statistical analysis was performed using 2-tailed Student's t test. Statistical significance was defined as $P < 0.05$.

Study approval

Handling and breeding of mice and rats and all experiments were performed in accordance with the German laws for animal protections and were approved by the local animal care committee (Landesamt für Natur, Umwelt und Verbraucherschutz Nordrhein-Westfalen, Recklinghausen, Germany) and the Bezirksregierung Köln. For human tissue samples, the study protocol for tissue donation was approved by the Ethics Committee of the University of Giessen in accordance with national law and with Good Clinical Practice/International Conference on Harmonisation guidelines. Written informed consent was obtained from each patient or the patient's next of kin.

Results

p110 α deficiency in SMCs promotes AAA formation in PPE treated mice

To investigate if p110 α signaling might be implicated in human pathogenesis, we analyzed gene expression of PIK3CA (p110 α) and the most important up-stream growth factor PDGF-B (**Figure 1A, B**). Whereas PIK3CA is not regulated in AAA, PDGF-B is significantly up-regulated, indicating increased PI3K activation in diseased tissue. To investigate the impact of p110 α in SMCs on AAA formation, we used sm-p110 $\alpha^{-/-}$ mice in the PPE model of AAA formation (**Figure 1C**). Similar to the situation in human AAA patients, AAA induction via PPE infusion into the infrarenal segment of the aorta led to an activation of PI3K signaling in the medial compartment as monitored by phosphorylation of AKT (**Figure 1D**). This response was diminished in sm-p110 $\alpha^{-/-}$ mice, demonstrating the importance of p110 α for AAA induced PI3K signaling in medial SMCs. Further investigation of AAA formation in sm-p110 $\alpha^{-/-}$ mice and sm-p110 $\alpha^{+/+}$ controls revealed substantially increased AAA growth in sm-p110 $\alpha^{-/-}$ mice (**Figure 1E, F**). The incidence of AAA disease (>50% increase of lumen diameter) was higher in sm-p110 $\alpha^{-/-}$ mice (67% versus 30%), and the increase of the aortic diameter significantly elevated (**Figure 1G, H**). In addition, PPE induced AAA formation was accompanied by infiltration of MOMA2⁺ macrophages into the aortic media. This inflammatory response was significantly more pronounced in sm-p110 $\alpha^{-/-}$ mice (**Figure 1I**). These data indicate that p110 α deficiency in SMCs promotes AAA formation and vascular inflammation. Lack of p110 α expression may affect AAA formation in two ways: It might predispose mice to develop AAA disease due to preexisting structural alterations in the aortic wall, and/or it might promote disease progression after PPE perfusion via altering protective SMC functions.

p110 α deficiency impairs aortic wall structure and function

Therefore, we next investigated the impact of p110 α deficiency in SMCs on aortic structure and function in more detail. sm-p110 $\alpha^{-/-}$ mice are characterized by a reduced media area under basal conditions compared to WT controls which likely reflects an impaired capacity of p110 $\alpha^{-/-}$ SMCs to proliferate and migrate during aortic development (**Figure 2A**). Analysis of the ultrastructure revealed that aortae from sm-p110 $\alpha^{-/-}$ mice are characterized by severe derangements of the medial compartment, harbouring detached SMCs, impaired elastic lamellae, and features of apoptotic cell death including fragmented nuclei and swollen

mitochondria (**Figure 2B, C**). To determine whether the impaired aortic wall structure observed in knock out mice correlates with altered vascular function, we investigated contractility of abdominal aorta derived from sm-p110 α ^{-/-} mice and sm-p110 α ^{+/+} controls using wire myography. Aortic rings isolated from sm-p110 α ^{-/-} mice displayed significantly less relaxation in response to stimulation of endothelial nitric oxide (NO) production (**Figure 2D**). The dose response relationship in knock out aortae to the NO donor nitroglyceride was also significantly altered (**Figure 2E**), indicating that this effect was endothelium independent and probably due to an impairment of SMC function.

The reduced contractility of sm-p110 α ^{-/-} explants could be related to an impaired contractile phenotype of p110 α ^{-/-} SMCs. This prompted us to investigate the expression of contractile markers in the aortic wall. A bulk RNAseq approach demonstrated that numerous contractile SMC marker genes were significantly downregulated in sm-p110 α ^{-/-} aortae compared to wild type controls (**Figure 3A**). Western blot analysis revealed that protein expression of calponin and myosin heavy chain (MHC) was significantly decreased in sm-p110 α ^{-/-} aortae, while the expression of α -actin remained unchanged (**Figure 3B**). This finding was also confirmed by immunohistochemical and immunofluorescence staining (**Figure 3C, D, E**). Interestingly, SMCs isolated from sm-p110 α ^{-/-} mice express less α -actin in cell culture (**Figure 3F**). This could indicate compensatory mechanisms in the aortic wall to increase α -actin expression in sm-p110 α ^{-/-} mice.

In addition to SMCs, the ECM also significantly contributes to aortic wall structure and function. In particular, elastic fibers play a major role in maintaining the biomechanical properties of the aortic wall. p110 α deficiency in SMCs caused increased number of elastic fiber breaks in the thoracic segment of the aorta, whereas the abdominal aorta was not affected under basal conditions (**Figure 4A**). To explore the impact of p110 α deficiency on cellular function, we isolated SMCs from sm-p110 α ^{-/-} and sm-p110 α ^{+/+} mice. Interestingly, p110 α ^{-/-} SMCs produced less tropoelastin than wild type control cells, whereas fibrillin-1 expression was unaffected (**Figure 4B**). These data indicates that disturbed elastin homeostasis in p110 α ^{-/-} SMCs might be a prerequisite for elastic fiber breaks. Collagen represents another ECM component which confers vascular stiffness. Analysis of collagen expression by Picro Sirius Red staining in aortae from sm-p110 α ^{-/-} mice and sm-p110 α ^{+/+} controls revealed slightly increased collagen amounts in the thoracic segment of elder animals, however, without reaching significance (**Figure 4C**).

Further matrix analysis of ECM fibers on isolated SMCs stained by immunofluorescence should reveal the effects of an altered ECM expression on the respective fibre structure. Quantitative analysis of alignment, fiber width, and fiber length revealed that elastin fibers from p110 α deficient SMCs are significantly shorter than those from control cells, whereas fibrillin fiber dimensions were not compromised (**Figure 5A, B**). In addition, we found a significantly increased alignment coefficient of collagen fibers indicating highly ordered structures of that fiber network potentially promoting stiffness (**Figure 5C**).

Taken together, both aortic wall structure and function in sm-p110 α ^{-/-} mice were impaired. In this context, reduced expression of marker genes of the contractile SMC phenotype was detected in p110 α deficient cells, and elastin homeostasis was also impaired. Collectively, these data suggest that a preexisting vascular disorder may have at least partially caused the diseased phenotype.

p110 α deficiency impairs vascular remodeling and promotes elastic fiber degradation in AAA

We next investigated alterations in the abdominal aortic wall in PPE treated sm-p110 α ^{-/-} and sm-p110 α ^{+/+} mice. Destruction of the ECM peaked 28 days after PPE infusion in both wild type controls and sm-p110 α ^{-/-} mice. However, in sm-p110 α ^{-/-} mice elastic fiber degeneration already started earlier than in sm-p110 α ^{+/+} mice (**Figure 6A**). In contrast to the situation under basal conditions, sm-p110 α ^{-/-} mice displayed more elastic fiber breaks than control mice 3 days after PPE perfusion of the infrarenal abdominal segment (**Figure 6B**). In parallel to the increased occurrence of strand breaks, an increased expression of matrix metalloproteinases (MMPs) upregulated in AAAs such as MMP-2 and MMP-9 was measured after PPE infusion. However, the increased strand breaks in the knock out animals cannot be attributed to a differential MMP expression, as they are expressed at similar levels than in the control animals (**Figure 6C**).

AAA formation is characterized by loss of SMCs in the media compartment. Regenerative capacities of the aorta therefore depend on the ability of the vessel to compensate for this cell loss, for example through SMC proliferation. Consequently, the compromised aortic segment is characterized by an initial loss of SMCs 3 days after PPE infusion indicated by a sharply decreasing cellularity in the aortic wall and subsequent gradually increasing vessel wall recovery, media hypertrophy, and neointima formation in sm-p110 α ^{+/+} and sm-p110 α ^{-/-} mice.

However, this response is less pronounced in *sm-p110 α ^{-/-}* mice (**Figure 7 A-C**). PCNA staining reveal that proliferation of aortic cells is significantly reduced in *sm-p110 α ^{-/-}* mice (**Figure 7D**). This finding goes along with decreased cellular growth of isolated aortic SMCs from *sm-p110 α ^{-/-}* mice compared to wild type controls (**Figure 7E**). These data indicate that p110 α signaling contributes to SMC proliferation in the aortic wall and therefore to vascular recovery and remodeling after PPE infusion.

Lack of p110 α expression aggravated SMC proliferation by diminishing FOXO1 phosphorylation

To elucidate relevant p110 α mediated signaling events in more detail, we stimulated aortic SMCs from *sm-p110 α ^{-/-}* and *sm-p110 α ^{+/+}* mice with PDGF-BB. Growth factor stimulation of p110 α ^{+/+} cells rapidly induced phosphorylation of numerous signaling molecules downstream of PI3K such as AKT (including AKT1 and AKT2), Forkhead Box O (FOXO) transcription factors (FOXO1, FOXO3, FOXO4), and glycogen synthase kinase 3 β (GSK3 β). This response was significantly reduced in p110 α ^{-/-} SMCs (**Figure 8A**). Application of insulin led to similar results (Supplementary Figure). These results again show that p110 α is the essential isoform mediating PI3K-induced signaling events downstream of growth factor receptors in SMCs. It was previously demonstrated that FOXOs are implicated in SMC dedifferentiation and proliferation. PI3K/AKT dependent phosphorylation of FOXOs results in their inhibition and nuclear exclusion. Here, we show that particularly FOXO1 is up-regulated in human AAA disease (**Figure 8B**). Therefore, we investigated the impact of FOXO1 inhibition of growth factor stimulated p110 α ^{-/-} SMCs and wild type control cells. p110 α deficiency significantly diminished PDGF induced SMC proliferation compared to wild type cells. However, proliferation of p110 α ^{-/-} SMCs was fully rescued by application of the specific FOXO1 inhibitor AS1842856, whereas FOXO1 inhibition had no effect on proliferation of PDGF stimulated wild type cells (**Figure 8C**). These data clearly demonstrate that p110 α mediated inactivation of FOXO1 is mechanistically responsible for PDGF induced SMC proliferation. Furthermore, siRNA mediated knockdown of FOXO1 increased tropoelastin as well as calponin expression in SMCs, suggesting that FOXO1 inactivation is important for phenotypic modulation and elastogenesis.

Discussion

The results reported herein demonstrate that loss of p110 α signaling in SMCs results in impaired aortic wall structure and function, contributing to exaggerated development of AAA in PPE treated mice. Thereby, features of sm-p110 α ^{-/-} mice resemble the situation in human AAA disease - morphologically, biomechanically and molecularly.

The aortic wall of AAA patients is characterized by decreased number of SMCs compared to the healthy vessel wall.^{25,26} SMC apoptosis is a major cause of SMC loss in AAA development.²⁷ Consequently, apoptotic SMCs have been frequently observed in the medial aortic wall of AAA.²⁸ Since p110 α mediates SMC survival,^{12, 13} lack of p110 α is expected to promote SMC death in the aortic wall. Consequently, sm-p110 α ^{-/-} mice exhibited aortae with reduced wall thickness and features of apoptotic cell death including fragmented nuclei and swollen mitochondria. In development and during vascular repair, SMCs express and secrete ECM proteins. Together with SMCs, elastic fibers, such as elastin, fibrillin and collagen, maintain structural and functional integrity of the aortic wall. The reduced SMC number in the diseased aortic wall impairs its abilities in producing connective tissue and repairing elastin fiber breaks, which promotes AAA formation.²⁶ Accordingly, ECM degradation occurs in AAA, contributing to rupture and dilation of the aortic wall. Consistent with the situation in human AAA patients, sm-p110 α ^{-/-} mice are characterized by disturbances in the aortic wall structure and impaired elastin fiber production. The interaction between SMCs and the ECM is essential for proper regulation of SMC functions, such as SMC contractility. Contractility was impaired in 23% of aortic tissues from AAA patients, suggesting that impaired SMC contractility plays a role in AAA pathophysiology. Consequently, SMCs of human AAA patients are characterized by an impaired contractility upon ionomycin stimulation compared with control SMC.²⁹ Again, many of these characteristics shown in AAA disease are recapitulated in sm-p110 α ^{-/-} mice: sm-p110 α ^{-/-} mice displayed reduced expression of contractile genes, such as calponin and myosin heavy chain, and decreased responsiveness to vasodilator NO.

All these impairments of the aortic wall structure and function show that p110 α serves important functions during development and/or maintenance of a functional aortic wall. Thereby, p110 α affects SMC proliferation, survival, and phenotypic modulation. For this reason, sm-p110 α ^{-/-} mice were expected to promote AAA progression. However, sm-p110 α ^{-/-} mice did not develop AAA disease under basal conditions. This finding suggests that the aortic wall shows a remarkable resilience. The preexisting vascular derangements have rather made

sm-p110 α ^{-/-} aortae prone to a second AAA promoting hit. Herein, we have chosen the PPE model, as it is widely accepted to be the best mimicry of human AAA disease.^{8,30} PPE induced AAA show a time-dependent pathogenesis with acute to chronic inflammation, and vascular wall remodelling.^{31,32} Many of these features resemble end stage human AAA disease.^{33,34} PPE infused aortae are characterized by increased expression of various MMPs along with massive infiltration of leukocytes suggesting a macrophage-dependent increased elastolysis and ECM turnover.³⁵ SMCs can also promote these processes through activation and modulation of MMPs.²⁶ Increased MMPs, in particular, MMP-2 and MMP-9, degrade the ECM, thereby weakening the vascular wall and leading to AAA formation. MMP-2 and MMP-9 were profoundly up-regulated in both sm-p110 α ^{-/-} and sm-p110 α ^{+/+} mice following PPE infusion. However, MMP-2 and MMP-9 expression were not differentially expressed. In sm-p110 α ^{-/-} mice, the MMPs encountered pre-damaged elastic fibers, which were presumably degraded more rapidly promoting enhanced AAA development in these mice. In addition, leukocyte derived cytokines, increased oxidative stress, and ECM breakdown promote SMC death, which should be further amplified in the absence of p110 α dependent survival signaling. Therefore, it is highly expected that pre-damaged sm-p110 α ^{-/-} aortae are more susceptible to PPE induced AAA. Consequently, the PPE mediated effects were more pronounced in sm-p110 α ^{-/-} mice compared to wild type controls yielding enhanced AAA development.

Our data also demonstrate that p110 α is not only responsible for maintaining vascular integrity, but also controls regenerative mechanisms that counteract aortic dilatation. To regenerate the compromised vessel segment, the loss of SMCs must be compensated by increased cell proliferation. SMC proliferation increases the cell number within the aortic wall and can therefore counteract AAA development. However, diminished proliferative capacity is seen in human AAA-derived SMC compared with non-aneurysmal SMC.⁹ An effective therapeutic strategy from this point of view could therefore be to promote proliferative capacities of SMCs. Herein, we demonstrated that p110 α signaling is a strong inducer of SMC proliferation which largely contributes to media regeneration and neointima formation. However, the impact of SMC proliferation on AAA development is controversially discussed. For example, mTOR-dependent proliferative SMCs promote dilatation and dissection of the aortic wall rather than prevent disease progression,³⁶ and inhibition of tyrosine kinase mediated SMC proliferation and phenotypic switching by lenvatinib ameliorates AAA formation.³⁷

However, proliferation of SMCs is associated with their dedifferentiation, which potentially exerts detrimental effects in AAA development rather than the proliferative response per se. Following vessel injury, SMCs undergo clonal expansion as demonstrated in angiotensin II-induced thoracic aortic aneurysm by using Myh11-CreERT2/Rosa26 Confetti mice. Thereby, proliferative SMCs showed a decreased expression of SMC markers and increased expression of phagocytic markers.³⁸ Further studies revealed that dedifferentiated SMCs exhibit phenotypes resembling those of mesenchymal stem cells, myofibroblasts, fibroblasts, osteogenic cells, chondrocytes, macrophage-like inflammatory cells, foam cells, or adipocyte-like cells, which might exert opposing functions in AAA disease.^{36,39,40} The most commonly reported phenotypic modulation observed in patients with AAA is the decreased expression of smooth muscle differentiation markers and increased expression of inflammatory proteins.⁴¹ Thus, subsets of dedifferentiated SMC phenotypes may promote the progression of AAA via decreased contractility as well as increased secretion of proinflammatory cytokines and MMPs. Therefore, it is important to dissect the precise stimuli responsible for SMC proliferation and accumulation in this context from those inducing detrimental dedifferentiated phenotypes to reveal potential new therapeutic targets. Importantly, although proliferation and phenotypic switching of SMCs are tightly coupled, they can be regulated by different signaling pathways. The expression of SMC contractile proteins is controlled by transcription factors, including myocardin.⁴² Myocardin forms a complex with the DNA-binding transcription factor serum response factor (SRF), which binds the CArG-boxes on SMC gene promoters and constitutes a docking platform for the myocardin-mediated transcription of target genes. Transcription factors, such as Kruppel-like factor 4 (KLF-4) and FOXO4, induce SMC phenotype switching by interfering with myocardin mediated transcriptional activity, subsequently suppressing the expression of genes encoding SMC contractile proteins.^{43,44} Consequently, inactivation of KLF4 or FOXO4 signaling ameliorates AAA formation in mice.^{44,45} Interestingly, KLF4 deficiency largely prevents SMC phenotypic modulation without inhibiting SMC proliferation⁴⁶ suggesting that proliferation and dedifferentiation can be regulated independently. In fact, we demonstrated that lack of p110 α expression in SMCs impaired SMC proliferation without promoting SMC dedifferentiation as both MMP expression in AAA and PDGF induced induction of KLF4 in SMCs (not shown) were not affected by p110 α knockout. In contrast, contractile proteins such as calponin and myosin heavy chain are downregulated in sm-p110 α ^{-/-} mice, indicating that p110 α signaling rather

promotes the contractile SMC phenotype. These data suggest that growth factors/RTKs regulate SMC proliferation and dedifferentiation via distinct pathways, respectively. Whereas induction of KLF4 regulates phenotypic modulation³⁹, activation of p110 α induces SMC proliferation.

We identified p110 α dependent phosphorylation of FOXO1 as the crucial downstream event for SMC proliferation as specific inhibition of FOXO1 completely rescued the anti-proliferative p110 α ^{-/-} phenotype without affecting proliferation of wild type cells. Interestingly, 50% reduction of FOXO1 expression was sufficient to significantly increase the expression of calponin and elastin, indicating that FOXO1 promotes SMC dedifferentiation, too. Furthermore, FOXO1 is significantly upregulated in human AAA disease. The role of FOXO in SMCs is not well understood so far. It is suggested that PI3K/AKT dependent phosphorylation of FOXO1 mediates downregulation of the cell cycle inhibitor p27kip thereby promoting cellular proliferation.⁴⁷ In endothelial cells, FOXO1 regulates both metabolic and proliferative events. Specifically, FOXO1 overexpression suppresses Myc signaling and thereby impairs glycolysis, mitochondrial function, and also the proliferation of endothelial cells,⁴⁸ suggesting that FOXO1 might serve similar functions in SMCs. It is likely that activation of FOXO3 and FOXO4 contributes to the sm-p110 α ^{-/-} phenotype, too, as it was shown that inactivation of FOXO3 as well as FOXO4 protects against aortic aneurysm formation^{24,44}, and we demonstrated herein that FOXO3 and FOXO4 phosphorylation and thus inactivation were reduced in p110 α ^{-/-} SMCs.

In conclusion, our data demonstrate that p110 α signaling promotes vascular integrity and regeneration in healthy and diseased aorta by maintaining contractility, elastogenesis, and proliferative capacities of aortic SMCs. Importantly, activation of p110 α /FOXO signaling allows to specifically induce SMC proliferation without promoting dedifferentiation which might be of particular importance to treat late stage AAA. The impact of p110 α signaling on vascular integrity is clinically relevant in the context of current approaches aimed at p110 α inhibition for cancer therapy. Since specific FOXO inhibitors are readily available⁴⁹ and p110 α activators are under development, the findings presented herein might also pave the road to develop new therapeutic strategies to treat AAA disease.

Acknowledgements

The technical help by Frank Oberhäuser and Maximilian Becker is greatly acknowledged. This work contains part of a doctoral thesis by MS. LGF and DM were supported by the Deutsche Forschungsgemeinschaft (RTG-2407 to SR and SB).

Sources of funding

This work was supported by the Deutsche Forschungsgemeinschaft (project B06, TRR-259, to SR and MV).

Figure legends

Figure 1. Lack of p110 α in SMCs promotes AAA formation in mice. **A, B** mRNA expression of PIK3CA (p110 α) (A) and PDGFB (platelet-derived growth factor B-chain) (B) in human aortic samples from healthy controls (n=3) or AAA patients (n=12). **C** Porcine pancreatic elastase (PPE) is infused into the infrarenal segment of aortae in male sm-p110 $\alpha^{+/+}$ (n=10) and sm-p110 $\alpha^{-/-}$ (n=9) mice. Aortae are analyzed under baseline conditions as well as 3, 7, and 28 days after PPE intervention. **D** Representative immunohistochemical stainings showing AKT phosphorylation 3 days after PPE intervention in sm-p110 $\alpha^{-/-}$ and sm-p110 $\alpha^{+/+}$ mice compared to control. **E** Representative pictures of aortae from sm-p110 $\alpha^{+/+}$ and sm-p110 $\alpha^{-/-}$ mice demonstrate AAA formation 28 days after PPE infusion. **F** Analysis of ultrasound images of sm-p110 $\alpha^{-/-}$ and sm-p110 $\alpha^{+/+}$ mice revealed **(G)** elevated incidence for AAA (increase of lumen diameter >50%) and **(H)** significantly increased aortic diameter compared to sm-p110 $\alpha^{+/+}$ control mice. n=9-10. **I** Moma2 staining of sections from PPE and control sm-p110 $\alpha^{-/-}$ and sm-p110 $\alpha^{+/+}$ mice as indicated. N=3-7; ANOVA Tukey multiple comparison. Data are presented as means \pm S.D.

Figure 2. Impaired aortic wall structure and functionality in p110 $\alpha^{-/-}$ mice under basal conditions. **A** Representative HE histochemical staining of cross sections from the infrarenal part of the aorta and quantification of media thickness in sm-p110 $\alpha^{+/+}$ versus sm-p110 $\alpha^{-/-}$ mice under basal conditions, respectively (n=4-5). **B** Representative images of transmission electron microscopy of abdominal aortas from sm-p110 $\alpha^{+/+}$ and sm-p110 $\alpha^{-/-}$ mice demonstrating an intact media structure (top) and intact elastic fibers (below, indicated by the red arrow) in sm-p110 $\alpha^{+/+}$ mice (left) versus detached SMCs (top) and elastic fiber breaks (below, red arrow) in sm-p110 $\alpha^{-/-}$ mice (right) (2500 x magnification). **C** Intact mitochondria (top) and nuclei (below) (left) versus disturbed mitochondria (top) and fragmented nuclei (below) in (12000 x magnification) (right) are indicated by red arrows, respectively. **D, E** Relaxation of explanted abdominal aortic rings in response to acetylcholine (Ach, D) or nitroglycerin (NTG, E) was assessed by isometric force measurements and expressed as % of maximal prostaglandin F 2α -mediated constriction. * $p < 0.05$, ** $p < 0.01$. # $p < 0.001$; n=4, respectively. Data are presented as means \pm S.D

Figure 3. p110 α deficiency in SMCs impairs AAA phenotypic modulation. **A** Bulk RNAseq approach demonstrating differentially expressed SMC marker genes (right). Heatmap on the left with 100 top regulated genes. Myh: Myosin 11; Tpm2: tropomyosin b; Smtn: Smoothelin; Cnn1: Calponin 1; Acta2: α -actin **B** Western blot (left) and densitometric analysis (right) of protein expression of p110 α and the differentiation markers α -actin, calponin and myosin heavy chain (MHC) in sm-p110 $\alpha^{+/+}$ and sm-p110 $\alpha^{-/-}$ aortae (n=3) under basal conditions demonstrating impaired SMC differentiation in sm-p110 $\alpha^{-/-}$ aortae. RasGAP served as loading control. **C** Representative immunohistochemical calponin staining from sm-p110 $\alpha^{+/+}$ and sm-p110 $\alpha^{-/-}$ aortic cross-sections, respectively (scale bar = 50 μ m; n = 3) and quantification. **D** Representative immunohistochemical staining of cross-sections from the infrarenal part of sm-p110 $\alpha^{+/+}$ and sm-p110 $\alpha^{-/-}$ aortae under basal conditions using an antibody against α -actin (scale bar = 50 μ m; n = 3) and quantification. **E** Representative images of immunofluorescence stainings of α -actin (green) and elastinin (purple) using confocal microscopy on aortic sections from sm-p110 $\alpha^{+/+}$ versus sm-p110 $\alpha^{-/-}$ mice. **F** Representative images of immunofluorescence stainings of α -actin (green) in sm-p110 $\alpha^{+/+}$ versus sm-p110 $\alpha^{-/-}$ aortic SMCs.

Figure 4. Elastic fiber expression in aortae and SMCs from sm-p110 $\alpha^{-/-}$ mice. **A** Representative images of elastic van Gieson stainings (100 x and 400 x magnification) in cross section from thoracic (top) versus abdominal aorta (bottom) from sm-p110 $\alpha^{+/+}$ versus sm-p110 $\alpha^{-/-}$ mice under basal conditions. Quantifications of elastic fiber breaks, respectively, are shown on the right (n=5, respectively). **B** Western blots (left) and densitometrical analysis (right) demonstrating expression of elastin (top) and fibrillin (bottom) in SMCs from sm-p110 $\alpha^{+/+}$ and sm-p110 $\alpha^{-/-}$ mice. RasGap and β -actin served as loading controls. **C** Representative Picro Sirius Red stainings for collagen of cross-sections from abdominal and thoracic aortae from 12 or 24 weeks old sm-p110 $\alpha^{+/+}$ and sm-p110 $\alpha^{-/-}$ mice as indicated. (n=3-5). Collagen was quantified.

Figure 5: Analysis of fiber length, width and alignment of elastic fiber matrices. Aortic SMCs isolated from Col19a1 wildtype (+/+) and null (N/N) mice were grown to confluence for 7d. Resultant elastin (**A**), fibrillin (**B**) and collagen (**C**) matrices were stained by immunofluorescence (representative images are shown in the first row (top), respectively).

Fibrillar collagen alignment was quantified using CurveAlign/CT-FIRE. Second row: Images generated by CurveAlign showing the location (red dots) and orientation (green lines) of extracted fibers. Third row: Heatmaps indicating regional fiber alignment (red denotes areas of greater alignment). Fourth row: CT-FIRE extracted fibers overlaid on master image (first row). Information for entire fibers are shown and highlighted by different colored lines for contrast. Graphs illustrate mean fibrillar alignment, width, and length \pm S.D. in wildtype as indicated. Statistics: Data normality was assessed using the Shapiro–Wilk test. Alignment coefficient data were analyzed by an unpaired, two-tailed Student's T-test. Data in fiber width and fiber length were analyzed using the non-parametric Mann–Whitney U test, respectively. $p < 0.05$ was considered statistically significant.

Figure 6. Increased elastic fiber breaks in PPE treated sm-p110 α ^{-/-} mice. **A** Representative images of elastic van Gieson stainings (100 x and 400 x magnification) in cross sections from sm-p110 α ^{+/+} versus sm-p110 α ^{-/-} mice either under basal conditions or 3, 7, and 28 days after PPE perfusion and categorization of elastic fiber breaks (below). mean \pm S.D., n = 3-7. **B** Representative elastic van Gieson stainings and quantification of elastic fiber breaks in sm-p110 α ^{+/+} versus sm-p110 α ^{-/-} mice 3 days after PPE perfusion. mean \pm S.D., n = 3-7. **C** mRNA expression of MMP-2 and MMP-9 in AAA from sm-p110 α ^{+/+} versus sm-p110 α ^{-/-} mice 7 days after PPE perfusion determined by quantitative PCR. Data are presented as means \pm S.D..

Figure 7. Impaired vascular remodeling in PPE treated sm-p110 α ^{-/-} mice. **A** Medial hypertrophy, neointima formation and cellularity in the medial compartment were analyzed in hematoxylin / eosin stained cross sections of abdominal aortae from sm-p110 α ^{+/+} versus sm-p110 α ^{-/-} mice 0, 3, 7, and 28 days after PPE perfusion. **B** Quantification of the media/neointima area (n=3 mice, respectively). **C** Cellularity of indicated mice and periods of time. (n=3 mice, respectively). **D** Analysis of proliferating cells in the media/neointima compartment. Sections from mice were stained for PCNA 3 days post PPE perfusion. PCNA+ cells were quantified in media and neointima compartments (n=3-4). **E** Analysis of SMC proliferation. Growing curves of aortic cells isolated from sm-p110 α ^{+/+} and sm-p110 α ^{-/-} mice (n=2, respectively). Data are presented as means \pm S.D..

Figure 8. p110 α deficiency impairs FOXO signaling. **A** Representative Western blots of cultured SMCs detecting phosphorylated signaling proteins downstream of p110 α as indicated. Densitometrical analyses are shown on the right. (n=3-4). * $p < 0.05$, ** $p < 0.01$. # $p < 0.001$. **B** mRNA expression of FOXO transcription factors in human AAA (orange) versus healthy controls (green) as indicated; n=3-12. **C** PDGF-BB (50ng/ml) dependent SMC proliferation in p110 $\alpha^{-/-}$ SMCs and WT controls in the absence or presence of the FOXO1 specific inhibitor AS1842856 (AS, 1 μ M). n=5. **F** mRNA expression of Foxo1, Cnn1 (calponin), eln (elastin), and Col1a1 (collagen 1) in SMCs after knockdown of FOXO1 by four different siRNAs or in the presence of four different unrelated siRNAs as control determined by quantitative PCR. mean \pm S.D.

References

1. Kent KC. Clinical practice. Abdominal aortic aneurysms. *The New England journal of medicine*. 2014;371:2101-8.
2. Golledge J. Abdominal aortic aneurysm: update on pathogenesis and medical treatments. *Nat Rev Cardiol*. 2019;16:225-242.
3. Li X, Zhao G, Zhang J, Duan Z and Xin S. Prevalence and trends of the abdominal aortic aneurysms epidemic in general population--a meta-analysis. *PloS one*. 2013;8:e81260.
4. Bossone E and Eagle KA. Epidemiology and management of aortic disease: aortic aneurysms and acute aortic syndromes. *Nat Rev Cardiol*. 2021;18:331-348.
5. Golledge J and Norman PE. Current status of medical management for abdominal aortic aneurysm. *Atherosclerosis*. 2011;217:57-63.
6. Lloyd-Jones D, Adams R, Carnethon M, De Simone G, Ferguson TB, Flegal K, Ford E, Furie K, Go A, Greenlund K, Haase N, Hailpern S, Ho M, Howard V, Kissela B, Kittner S, Lackland D, Lisabeth L, Marelli A, McDermott M, Meigs J, Mozaffarian D, Nichol G, O'Donnell C, Roger V, Rosamond W, Sacco R, Sorlie P, Stafford R, Steinberger J, Thom T, Wasserthiel-Smoller S, Wong N, Wylie-Rosett J, Hong Y, American Heart Association Statistics C and Stroke Statistics S. Heart disease and stroke statistics--2009 update: a report from the American Heart Association Statistics Committee and Stroke Statistics Subcommittee. *Circulation*. 2009;119:e21-181.
7. Golledge J, Muller J, Daugherty A and Norman P. Abdominal aortic aneurysm: pathogenesis and implications for management. *Arteriosclerosis, thrombosis, and vascular biology*. 2006;26:2605-13.
8. Busch A, Bleichert S, Ibrahim N, Wortmann M, Eckstein HH, Brostjan C, Wagenhauser MU, Goergen CJ and Maegdefessel L. Translating mouse models of abdominal aortic aneurysm to the translational needs of vascular surgery. *JVS-vascular science*. 2021;2:219-234.
9. Rombouts KB, van Merrienboer TAR, Ket JCF, Bogunovic N, van der Velden J and Yeung KK. The role of vascular smooth muscle cells in the development of aortic aneurysms and dissections. *European journal of clinical investigation*. 2021:e13697.
10. Harkness ML, Harkness RD and Mc DD. The collagen and elastin content of the arterial wall. *The Journal of physiology*. 1955;127:33-4P.
11. Hellenthal FA, Buurman WA, Wodzig WK and Schurink GW. Biomarkers of AAA progression. Part 1: extracellular matrix degeneration. *Nat Rev Cardiol*. 2009;6:464-74.
12. Berghausen EM, Janssen W, Vantler M, Gnatzy-Feik LL, Krause M, Behringer A, Joseph C, Zierden M, Freyhaus HT, Klinke A, Baldus S, Alcazar MA, Savai R, Pullamsetti SS, Wong DW, Boor P, Zhao JJ, Schermuly RT and Rosenkranz S. Disrupted PI3K subunit p110alpha signaling protects against pulmonary hypertension and reverses established disease in rodents. *J Clin Invest*. 2021;131.
13. Vantler M, Jesus J, Leppänen O, Scherner M, Berghausen EM, Mustafov L, Chen X, Kramer T, Zierden M, Gerhardt M, Ten Freyhaus H, Blaschke F, Sterner-Kock A, Baldus S, Zhao JJ and Rosenkranz S. Class IA Phosphatidylinositol 3-Kinase Isoform p110 α Mediates Vascular Remodeling. *Arteriosclerosis, thrombosis, and vascular biology*. 2015;35:1434-44.
14. Bilanges B, Posor Y and Vanhaesebroeck B. PI3K isoforms in cell signalling and vesicle trafficking. *Nature reviews Molecular cell biology*. 2019;20:515-534.
15. Thorpe LM, Yuzugullu H and Zhao JJ. PI3K in cancer: divergent roles of isoforms, modes of activation and therapeutic targeting. *Nature reviews Cancer*. 2015;15:7-24.
16. Vanhaesebroeck B, Stephens L and Hawkins P. PI3K signalling: the path to discovery and understanding. *Nature reviews Molecular cell biology*. 2012;13:195-203.
17. Manning BD and Toker A. AKT/PKB Signaling: Navigating the Network. *Cell*. 2017;169:381-405.
18. Zhao JJ, Cheng H, Jia S, Wang L, Gjoerup OV, Mikami A and Roberts TM. The p110alpha isoform of PI3K is essential for proper growth factor signaling and oncogenic transformation. *Proceedings of the National Academy of Sciences of the United States of America*. 2006;103:16296-300.
19. Maegdefessel L, Spin JM, Raaz U, Eken SM, Toh R, Azuma J, Adam M, Nakagami F, Heymann HM, Chernogubova E, Jin H, Roy J, Hultgren R, Caidahl K, Schrepfer S, Hamsten A, Eriksson P, McConnell

- MV, Dalman RL and Tsao PS. miR-24 limits aortic vascular inflammation and murine abdominal aneurysm development. *Nature communications*. 2014;5:5214.
20. Klinke A, Berghausen E, Friedrichs K, Molz S, Lau D, Remane L, Berlin M, Kaltwasser C, Adam M, Mehrkens D, Mollenhauer M, Manchanda K, Ravekes T, Heresi GA, Aytekin M, Dweik RA, Hennigs JK, Kubala L, Michaelsson E, Rosenkranz S, Rudolph TK, Hazen SL, Klose H, Schermuly RT, Rudolph V and Baldus S. Myeloperoxidase aggravates pulmonary arterial hypertension by activation of vascular Rho-kinase. *JCI insight*. 2018;3.
 21. Sadri G, Fischer AG, Brittian KR, Elliott E, Nystoriak MA, Uchida S, Wysoczynski M, Leask A, Jones SP and Moore JBt. Collagen type XIX regulates cardiac extracellular matrix structure and ventricular function. *Matrix biology : journal of the International Society for Matrix Biology*. 2022;109:49-69.
 22. Li DY, Busch A, Jin H, Chernogubova E, Pelisek J, Karlsson J, Sennblad B, Liu S, Lao S, Hofmann P, Backlund A, Eken SM, Roy J, Eriksson P, Dacken B, Ramanujam D, Dueck A, Engelhardt S, Boon RA, Eckstein HH, Spin JM, Tsao PS and Maegdefessel L. H19 Induces Abdominal Aortic Aneurysm Development and Progression. *Circulation*. 2018;138:1551-1568.
 23. Rosenkranz S, DeMali KA, Gelderloos JA, Bazenet C and Kazlauskas A. Identification of the receptor-associated signaling enzymes that are required for platelet-derived growth factor-AA-dependent chemotaxis and DNA synthesis. *The Journal of biological chemistry*. 1999;274:28335-43.
 24. Lu W, Zhou Y, Zeng S, Zhong L, Zhou S, Song H, Ding R, Zhong G, Li Q, Hu Y, Wen Z, Liao Q, Wang Y, Lyu L, Zhong Y, Hu G, Liao Y, Xie D and Xie J. Loss of FoxO3a prevents aortic aneurysm formation through maintenance of VSMC homeostasis. *Cell death & disease*. 2021;12:378.
 25. Nordon IM, Hinchliffe RJ, Loftus IM and Thompson MM. Pathophysiology and epidemiology of abdominal aortic aneurysms. *Nat Rev Cardiol*. 2011;8:92-102.
 26. Qian G, Adeyanju O, Olajuyin A and Guo X. Abdominal Aortic Aneurysm Formation with a Focus on Vascular Smooth Muscle Cells. *Life*. 2022;12.
 27. Chakraborty A, Li Y, Zhang C, Li Y, LeMaire SA and Shen YH. Programmed cell death in aortic aneurysm and dissection: A potential therapeutic target. *Journal of molecular and cellular cardiology*. 2022;163:67-80.
 28. Rowe VL, Stevens SL, Reddick TT, Freeman MB, Donnell R, Carroll RC and Goldman MH. Vascular smooth muscle cell apoptosis in aneurysmal, occlusive, and normal human aortas. *Journal of vascular surgery*. 2000;31:567-76.
 29. Bogunovic N, Meekel JP, Micha D, Blankensteijn JD, Hordijk PL and Yeung KK. Impaired smooth muscle cell contractility as a novel concept of abdominal aortic aneurysm pathophysiology. *Scientific reports*. 2019;9:6837.
 30. Senemaud J, Caligiuri G, Etienne H, Delbosc S, Michel JB and Coscas R. Translational Relevance and Recent Advances of Animal Models of Abdominal Aortic Aneurysm. *Arteriosclerosis, thrombosis, and vascular biology*. 2017;37:401-410.
 31. Busch A, Holm A, Wagner N, Ergun S, Rosenfeld M, Otto C, Baur J, Kellersmann R and Lorenz U. Extra- and Intraluminal Elastase Induce Morphologically Distinct Abdominal Aortic Aneurysms in Mice and Thus Represent Specific Subtypes of Human Disease. *Journal of vascular research*. 2016;53:49-57.
 32. Busch A, Chernogubova E, Jin H, Meurer F, Eckstein HH, Kim M and Maegdefessel L. Four Surgical Modifications to the Classic Elastase Perfusion Aneurysm Model Enable Haemodynamic Alterations and Extended Elastase Perfusion. *European journal of vascular and endovascular surgery : the official journal of the European Society for Vascular Surgery*. 2018;56:102-109.
 33. Busch A, Hartmann E, Grimm C, Ergun S, Kickuth R, Otto C, Kellersmann R and Lorenz U. Heterogeneous histomorphology, yet homogeneous vascular smooth muscle cell dedifferentiation, characterize human aneurysm disease. *Journal of vascular surgery*. 2017;66:1553-1564 e6.
 34. Thompson RW, Curci JA, Ennis TL, Mao D, Pagano MB and Pham CT. Pathophysiology of abdominal aortic aneurysms: insights from the elastase-induced model in mice with different genetic backgrounds. *Annals of the New York Academy of Sciences*. 2006;1085:59-73.

35. Lu H, Du W, Ren L, Hamblin MH, Becker RC, Chen YE and Fan Y. Vascular Smooth Muscle Cells in Aortic Aneurysm: From Genetics to Mechanisms. *Journal of the American Heart Association*. 2021;10:e023601.
36. Li G, Wang M, Caulk AW, Cilfone NA, Gujja S, Qin L, Chen PY, Chen Z, Yousef S, Jiao Y, He C, Jiang B, Korneva A, Bersi MR, Wang G, Liu X, Mehta S, Geirsson A, Gulcher JR, Chittenden TW, Simons M, Humphrey JD and Tellides G. Chronic mTOR activation induces a degradative smooth muscle cell phenotype. *J Clin Invest*. 2020;130:1233-1251.
37. Busch A, Pauli J, Winski G, Bleichert S, Chernogubova E, Metschl S, Winter H, Trenner M, Wiegner A, Otto C, Fischer J, Reiser J, Werner J, Roy J, Brostjan C, Knappich C, Eckstein HH, Paloschi V and Maegdefessel L. Lenvatinib halts aortic aneurysm growth by restoring smooth muscle cell contractility. *JCI insight*. 2021;6.
38. Clement M, Chappell J, Raffort J, Lareyre F, Vandestienne M, Taylor AL, Finigan A, Harrison J, Bennett MR, Bruneval P, Taleb S, Jorgensen HF and Mallat Z. Vascular Smooth Muscle Cell Plasticity and Autophagy in Dissecting Aortic Aneurysms. *Arteriosclerosis, thrombosis, and vascular biology*. 2019;39:1149-1159.
39. Yap C, Mieremet A, de Vries CJM, Micha D and de Waard V. Six Shades of Vascular Smooth Muscle Cells Illuminated by KLF4 (Kruppel-Like Factor 4). *Arteriosclerosis, thrombosis, and vascular biology*. 2021;41:2693-2707.
40. Chen PY, Qin L, Li G, Malagon-Lopez J, Wang Z, Bergaya S, Gujja S, Caulk AW, Murtada SI, Zhang X, Zhuang ZW, Rao DA, Wang G, Tobiasova Z, Jiang B, Montgomery RR, Sun L, Sun H, Fisher EA, Gulcher JR, Fernandez-Hernando C, Humphrey JD, Tellides G, Chittenden TW and Simons M. Smooth Muscle Cell Reprogramming in Aortic Aneurysms. *Cell stem cell*. 2020;26:542-557 e11.
41. Shen YH, LeMaire SA, Webb NR, Cassis LA, Daugherty A and Lu HS. Aortic Aneurysms and Dissections Series. *Arteriosclerosis, thrombosis, and vascular biology*. 2020;40:e37-e46.
42. Kansakar U, Jankauskas SS, Gambardella J and Santulli G. Targeting the phenotypic switch of vascular smooth muscle cells to tackle atherosclerosis. *Atherosclerosis*. 2021;324:117-120.
43. Salmon M, Gomez D, Greene E, Shankman L and Owens GK. Cooperative binding of KLF4, pELK-1, and HDAC2 to a G/C repressor element in the SM22alpha promoter mediates transcriptional silencing during SMC phenotypic switching in vivo. *Circulation research*. 2012;111:685-96.
44. Zhao G, Fu Y, Cai Z, Yu F, Gong Z, Dai R, Hu Y, Zeng L, Xu Q and Kong W. Unspliced XBP1 Confers VSMC Homeostasis and Prevents Aortic Aneurysm Formation via FoxO4 Interaction. *Circulation research*. 2017;121:1331-1345.
45. Salmon M, Johnston WF, Woo A, Pope NH, Su G, Upchurch GR, Jr., Owens GK and Ailawadi G. KLF4 regulates abdominal aortic aneurysm morphology and deletion attenuates aneurysm formation. *Circulation*. 2013;128:S163-74.
46. Yoshida T, Kaestner KH and Owens GK. Conditional deletion of Kruppel-like factor 4 delays downregulation of smooth muscle cell differentiation markers but accelerates neointimal formation following vascular injury. *Circulation research*. 2008;102:1548-57.
47. Perrault R, Molnar P, Poole J and Zahradka P. PDGF-BB-mediated activation of CREB in vascular smooth muscle cells alters cell cycling via Rb, FoxO1 and p27(kip1). *Experimental cell research*. 2021;404:112612.
48. Wilhelm K, Happel K, Eelen G, Schoors S, Oellerich MF, Lim R, Zimmermann B, Aspalter IM, Franco CA, Boettger T, Braun T, Fruttiger M, Rajewsky K, Keller C, Bruning JC, Gerhardt H, Carmeliet P and Potente M. FOXO1 couples metabolic activity and growth state in the vascular endothelium. *Nature*. 2016;529:216-20.
49. Orea-Soufi A, Paik J, Braganca J, Donlon TA, Willcox BJ and Link W. FOXO transcription factors as therapeutic targets in human diseases. *Trends in pharmacological sciences*. 2022;43:1070-1084.

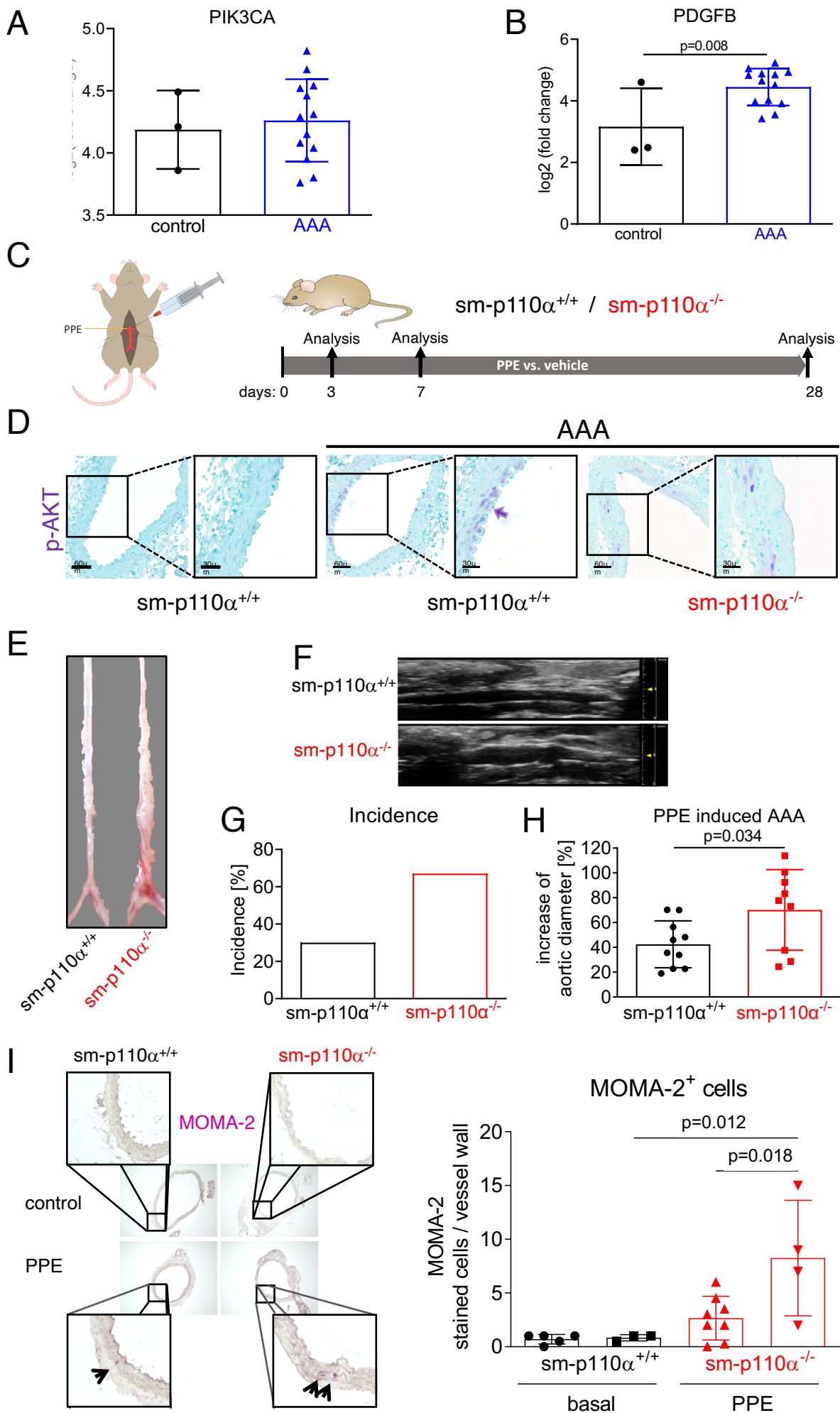


Figure 1: PPE induced AAA in *sm-p110α^{-/-}* mice

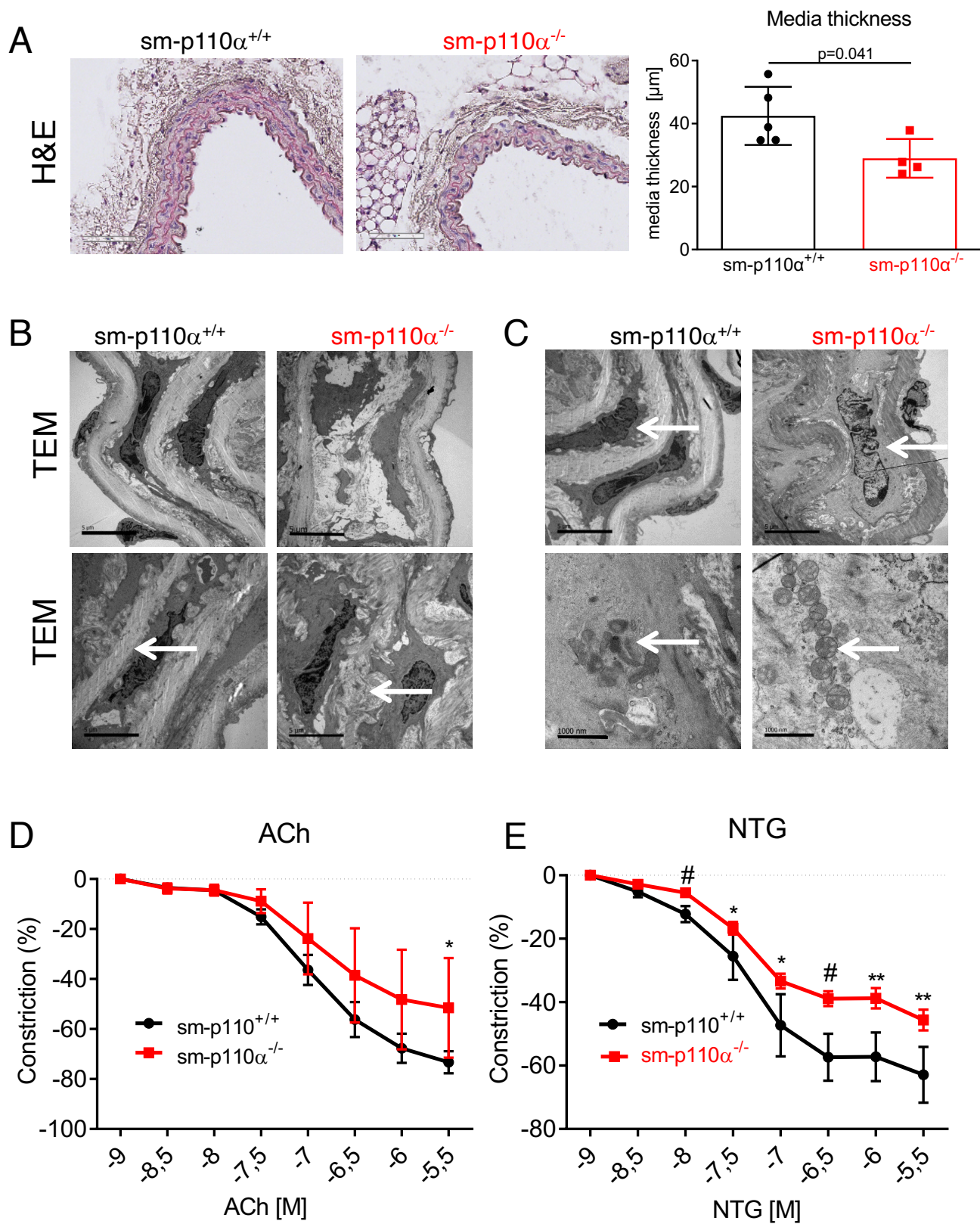


Figure 2. Impaired aortic wall structure and functionality in p110 $\alpha^{-/-}$ mice under basal conditions

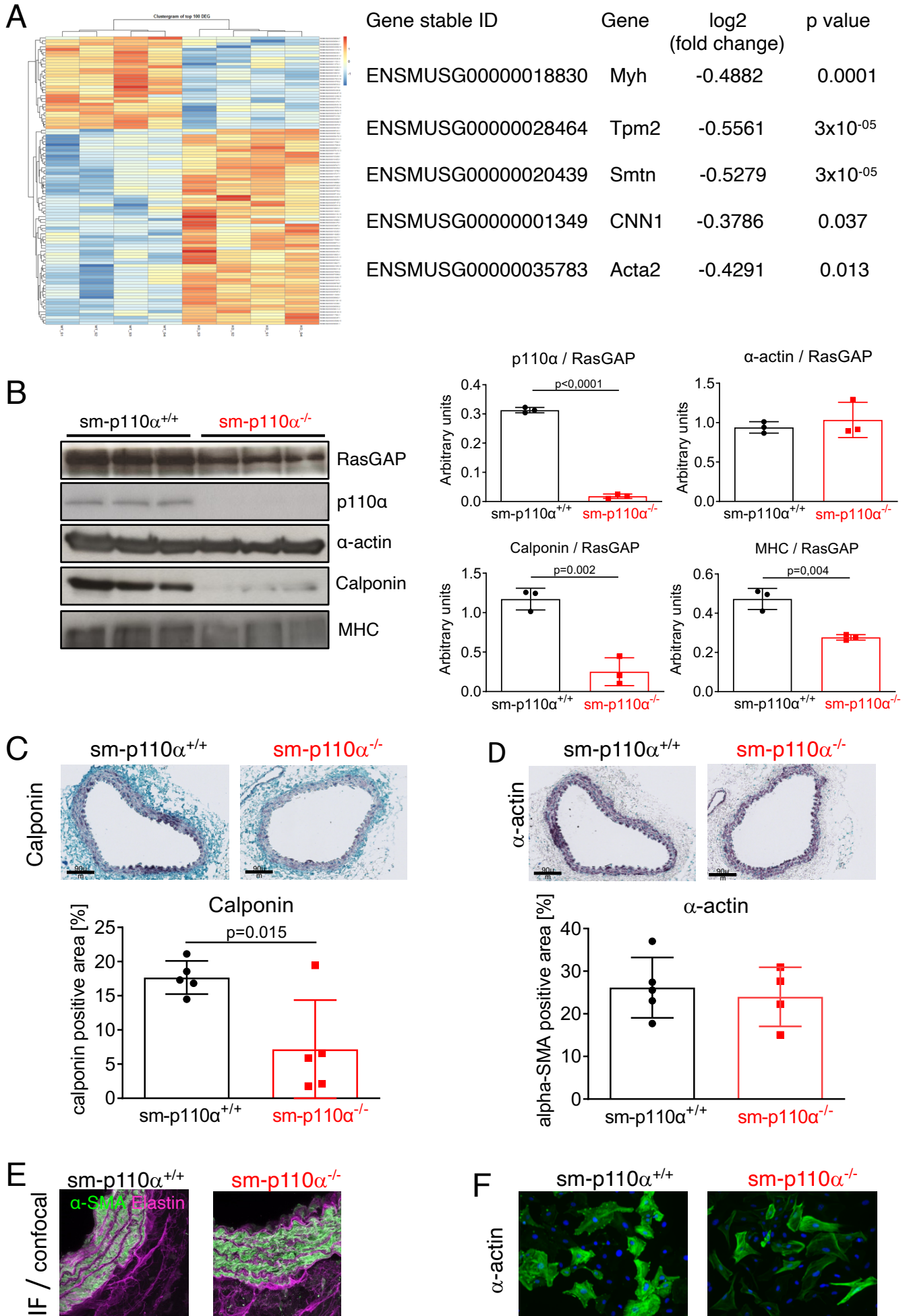


Figure 3. p110α deficiency impairs SMC differentiation.

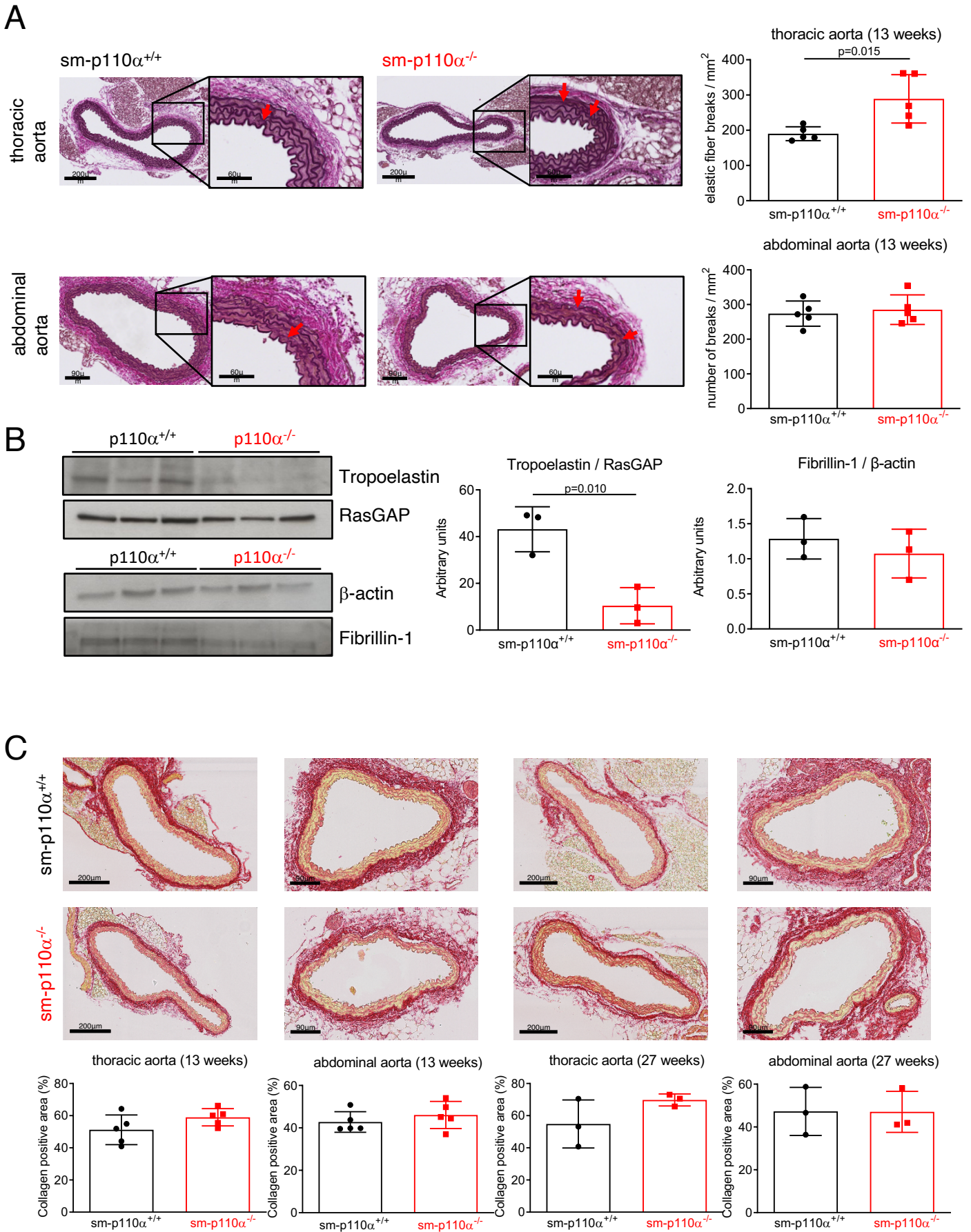


Figure 4: Elastic fiber homeostasis in aortae and SMCs

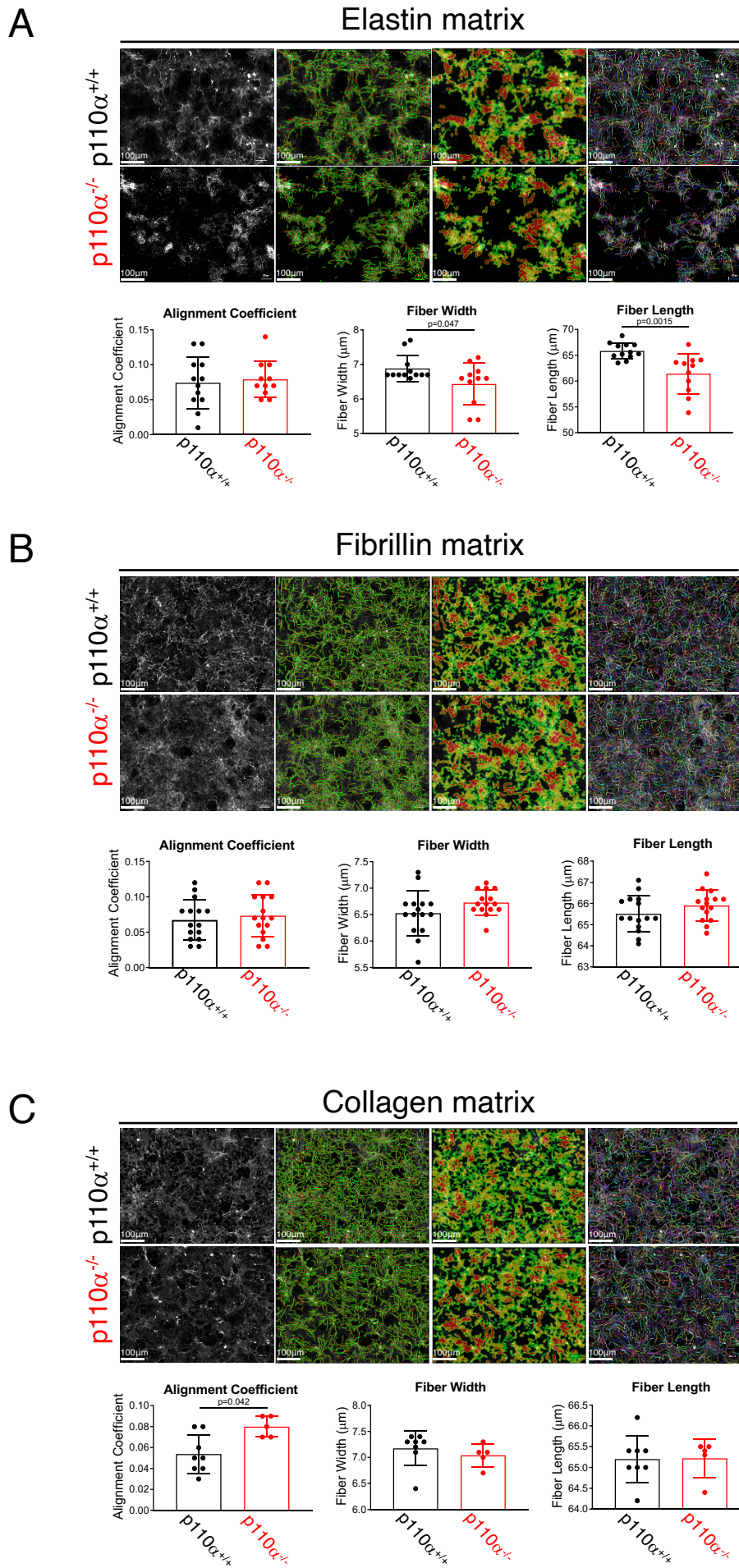
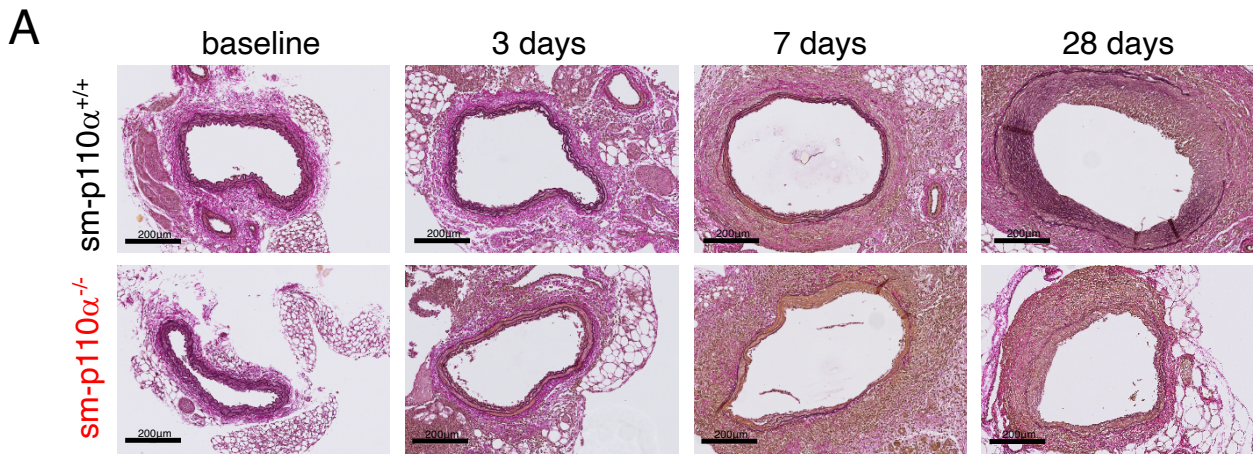


Figure 5: ECM fiber analyses in SMCs



Elastic fiber degradation

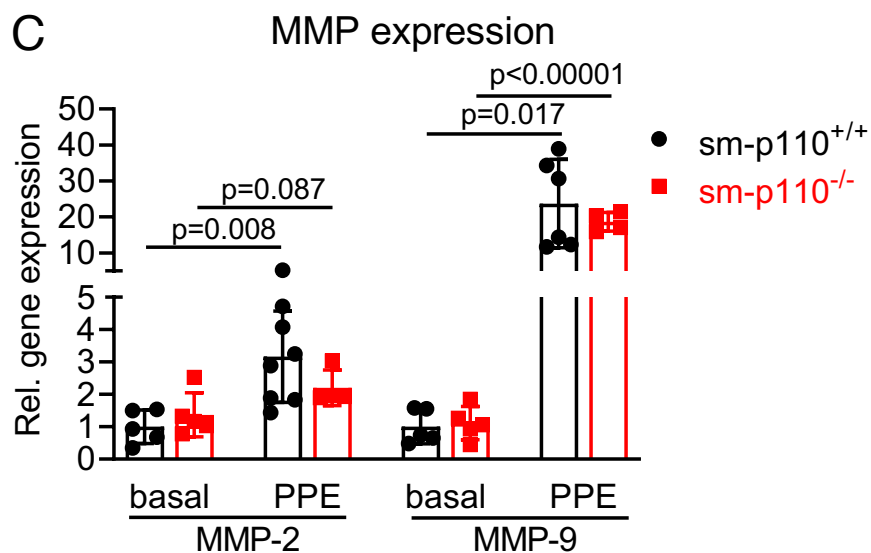
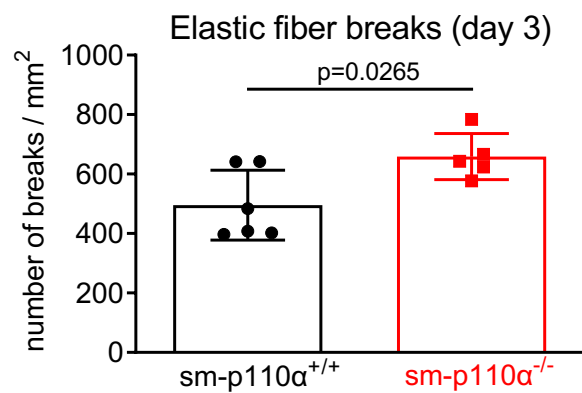
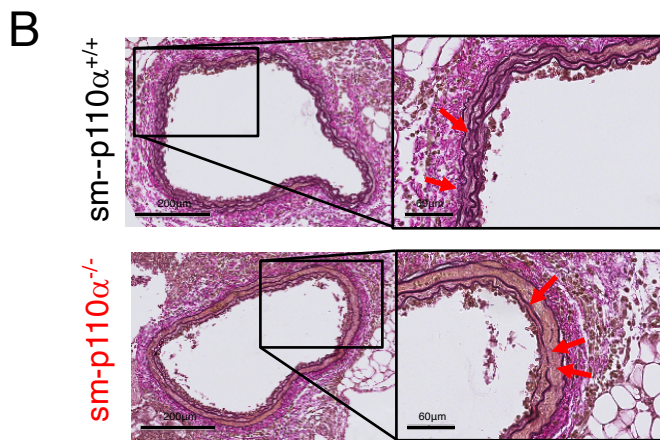
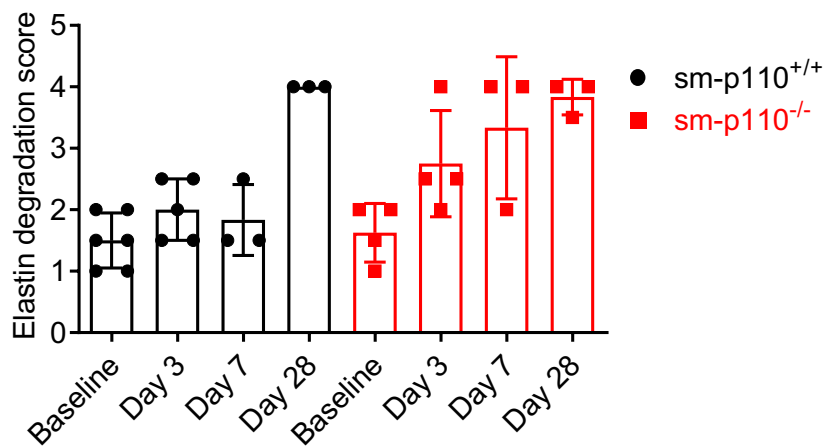


Figure 6: Increased elastic fiber breaks in PPE treated sm-p110 $\alpha^{-/-}$ mice

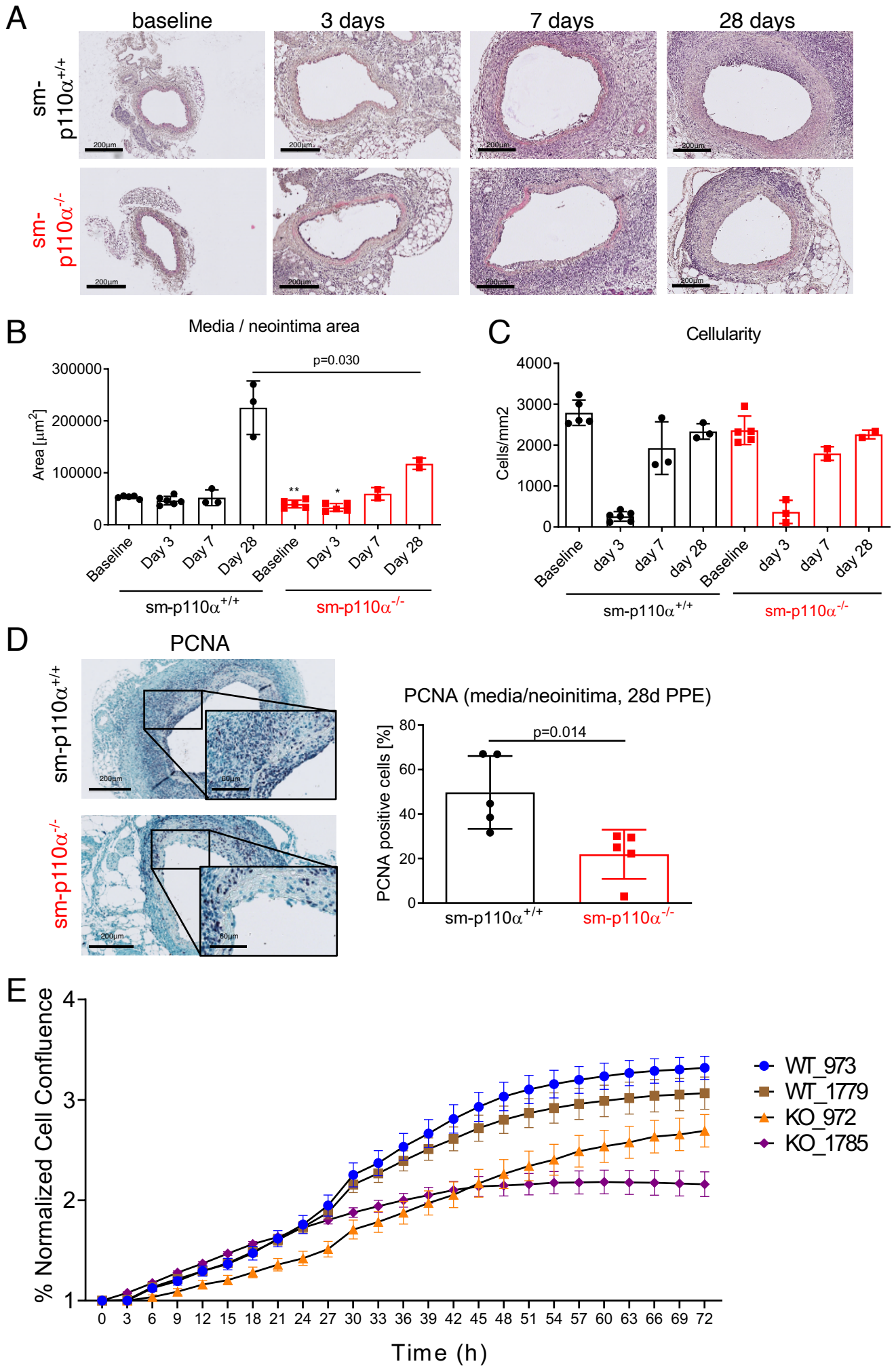


Figure 7: Impaired vascular remodeling in PPE treated sm-p110α^{-/-} mice

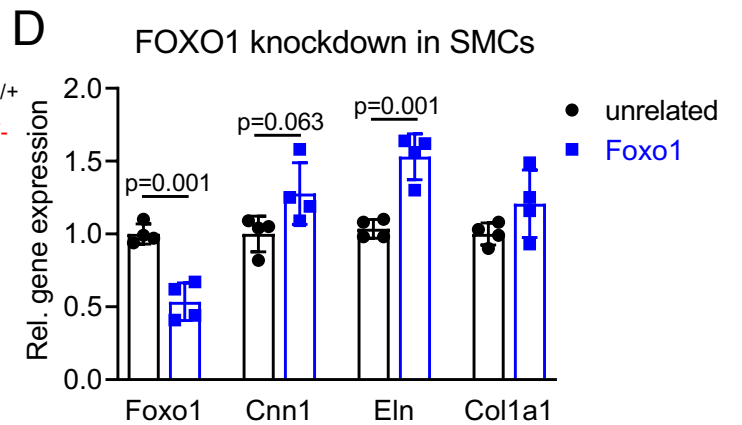
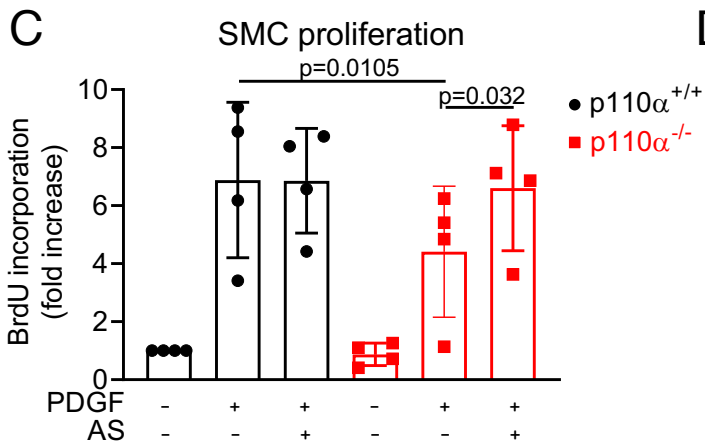
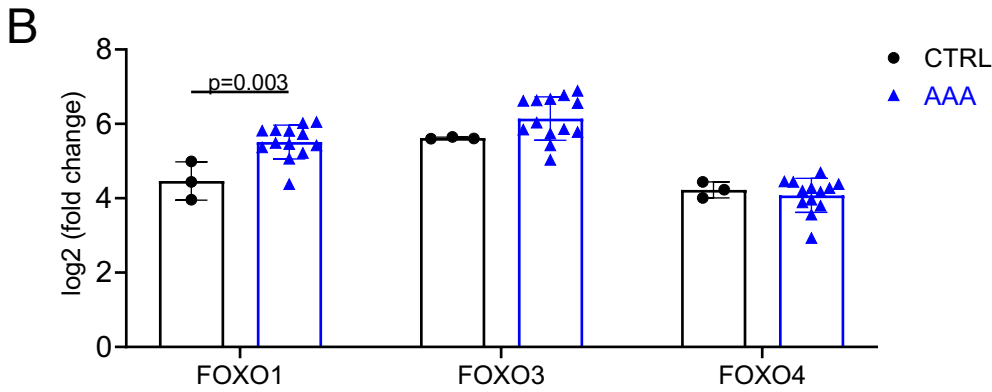
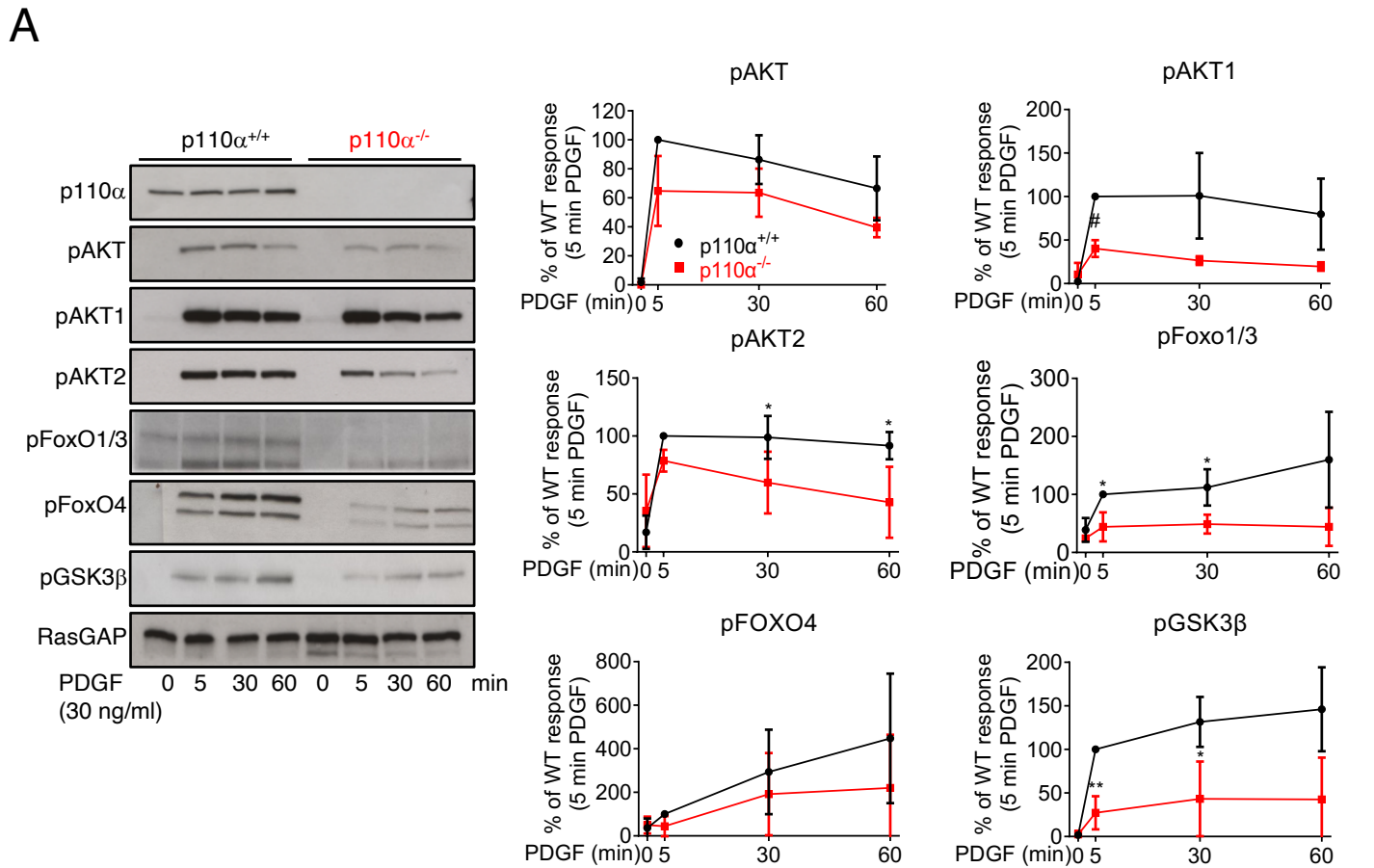


Figure 8: p110 α deficiency impairs FOXO signaling